Published in final edited form as:
Proteins. 2009 November 15; 77(3): 536–550. doi:10.1002/prot.22466.

On the Origin of the Catalytic power of Caboxypetidase A and Other Metalloenzymes

Alexandra Vardi Kilshtain and **Arieh Warshel***
Department of Chemistry, University of Southern California, 3620 McClintock Ave., Los Angeles, California 90089-1062

Abstract

Zinc metalloenzymes play a major role in key biological processes and Carboxypeptidase-A (CPA) is a major prototype of such enzymes. The present work quantifies the energetics of the catalytic reaction of CPA and its mutants using the EVB approach. The simulations allow us to quantify the origin of the catalytic power of this enzyme and to examine different mechanistic alternatives. The first step of the analysis used experimental information to determine the activation energy of each assumed mechanism of the reference reaction without the enzyme. The next step of the analysis involved EVB simulations of the reference reaction and then a calibration of the simulations by forcing them to reproduce the energetics of the reference reaction, in each assumed mechanism. The calibrated EVB was then used in systematic simulations of the catalytic reaction in the protein environment, without changing any parameter. The simulations reproduced the observed rate enhancement in two feasible general acid-general base mechanisms (GAGB-1 and GAGB-2), although the calculations with the GAGB-2 mechanism underestimated the catalytic effect in some treatments. We also reproduced the catalytic effect in the R127A mutant. The mutation calculations indicate that the GAGB-2 mechanism is significantly less likely than the GAGB-1 mechanism. It is also found, that the enzyme loses all its catalytic effect without the metal. This and earlier studies show that the catalytic effect of the metal is not some constant electrostatic effect, that can be assessed from gas phase studies, but a reflection of the dielectric effect of the specific environment.

Keywords

EVB; catalytic mechanism; general acid-general base; zinc; mutations; electrostatic effects

Introduction

Metalloenzymes play a major role in biology, ranging from mitochondrial O_2 reduction, destruction of O_2^- and H_2O_2, hydration of CO_2 to peptide bond cleavage, ester bond cleavage and hydrocarbon hydroxylation1. The general fact that the metal ions must provide a key catalytic role is well understood, but the exact way that this effect is exerted is less clear. For example, some works have emphasized the role of the metal in orienting the attacking water molecules or activating the nucleophile 2–5 other emphasized the role of the metal in stabilizing the transition state of the given reaction6–10.

The present work chose to explore this catalytic action of Carboxypeptidase A (CPA) as a prototype for metalloenzymes due in part to the role played by this enzyme in the history of metalloenzymes (see below).

*To whom correspondence should be addressed. warshel@usc.edu, Phone: 213-740-4114, Fax: 213-740-27.

CPA is a zinc metalloenzyme with a molecular weight of 35 kD that contains one zinc ion in its active site. CPA catalyses hydrolysis of terminal residues at the C-terminal of esteric and peptidic substrates. Carboxypeptidases were among the first proteases to be discovered. In 1929, Waldschmidt-Leitz and Purr found a protease in bovine pancrease that cleaved C-terminal amino acids from acylated peptides and named it carboxypolypeptidase 11. Several years later, it was purified and crystallized 12 and became known as “Anson’s enzyme”, and latter on it’s name was changed to carboxypeptidase A. Because it’s three-dimensional structure was already determined in 1960’s, CPA has been used as a model protein in studies of the structure and catalytic mechanism of metalloenzymes. Despite intensive investigation on CPA over several decades, structural and mechanistic models are still being refined by the use of more sophisticated x-ray crystallographic techniques, site directed mutagenesis and rapid kinetic analyses13.

Zinc metalloenzymes comprise a large family of enzymes with a wide variety of biological roles. These enzymes are characterized by the presence of at least one coordinated zinc ion as an essential catalytic component 14. Many of the zinc metalloenzymes are involved in disease conditions, and their inhibition is expected to block some damaging excessive activity. The best known zinc metalloenzyme is angiotensin converting enzyme (ACE). ACE is involved in blood pressure regulation 15, for which many inhibitors are already in clinical use. The first generation of ACE inhibitors was developed by Ondetti and Cushman 16 on the basis of comparisons of the ACE sequence and activity to the then known structure of CPA. These initial inhibitors were later developed into a few generations of efficient drugs for treating essential hypertension. Other important enzymes are enkephalinase which is active in neuropeptide processing 17, and matrix metalloenzymes (MMPs) which are involved in breast cancer 18. Their over-expression has also been linked with a variety of chronic diseases including arthritis 19, osteoporosis20, multiple sclerosis21, arteriosclerosis22, meningitis23, congestive heart failure24, liver cirrhosis25 and others.

Using structural information to elucidate the catalytic mechanism of these enzymes are necessary for better understanding of their function, and are essential for computer aided design of drugs by methods that are generally known as “Structure Based Drug Design”. Despite differences in folds, in zinc-binding motifs and in active site topologies, all of these enzymes have a catalytic zinc(II) ion at the active site where three of the coordination sites are occupied by protein ligands and the fourth coordination site is labile, and serves for binding of water, substrates and for catalysis 26،27. This resemblance between the different enzymes of the zinc metalloenzyme family suggests a similar catalytic mechanism 13،28،29. In fact, potent inhibitors of ACE 30 were developed on the basis of CPA inhibitors. Similarly, inhibitors of ACE were discovered to be good inhibitors of CPA 31.

Despite the availability of large amount of data from biochemical experiments and from X-ray structural studies of various zinc metalloenzymes, there is yet no agreement about the details of the catalytic mechanism of this family. Most of the attempts to elucidate this mechanism focused on CPA due to the extensive chemical/biochemical/structural work that will be briefly summarized below.

The structure of CPA was determined at a high resolution of 1.5Å (PDB codes:5cpa,1yme) 32،33. Recently, the structure of native CPA was solved at an even higher resolution of 1.25Å (PDB code:1m4l) 34. The active site (see Fig. 1) includes a zinc ion, coordinated to 3 protein ligands (His69, Glu72, and His196) and a water molecule. A nucleophile (Glu270) and an electrophile (Arg127) are located in a close proximity to the zinc ion and to the zinc bound water. Extraction of the zinc ion created an inactive enzyme, while a replacement of this ion by a range of dications resulted in diverse activities35. Crystallographic studies

suggested that Arg-127 is a key amino acid in the hydrolysis of peptides and esters by CPA. The guanidinium group of Arg-127 has been hypothesized to stabilize the gem-diol of the tetrahedral intermediate formed by the attack of a water molecule on the scissile carbonyl bond. Kinetic studies have shown that substitution of Arg-127 decreases k_{cat} for both esters and amide substrates, whereas K_m remain relatively unchanged; for R127M and R127A this corresponds to a kcal/mol decrease in the stabilization of the transition state of the rate-limiting step 36 .

The proposed mechanisms for CPA can be divided into two major types: 1) General-Acid-General-Base (GAGB) mechanisms ("Zn-hydroxide mechanism" or "water promoted pathway") in which a water molecule initially attacks the carbonyl while, or after, losing a proton. Overall the GAGB mechanism results in the formation of a gem-diol intermediate (Fig. 2A and Fig. 2B). 2) Direct nucleophilic attack (initially called "Zn-carbonyl mechanism" or "acyl pathway") on the peptide carbonyl by Glu270, resulting in the formation of an anhydride intermediate (Figure 3).

There are two suggested pathways for the GAGB mechanism. The first mechanism (GAGB-1) was suggested by Cristianson and Lipscomb13. This mechanism starts when a substrate binds to zinc but does not displace the zinc bound water, which is activated by zinc/Glu270 to perform a nucleophilic attack on the peptide carbonyl. The second stage of this mechanism involves an attack of the OH^- ion on the peptide carbonyl, and the formation of a gem-diol intermediate. The last stage involves a proton transfer from Glu270 to the peptide nitrogen, and a cleavage of the peptide bond. The detailed GAGB-1 mechanism is described in Figure 2(A).

The second mechanism (GAGB-2) was proposed by Mock37. This mechanism starts with a water attack on the carbonyl bond which is activated by the C-terminal of the substrate itself. The second stage of this mechanism involves an attack of the OH^- ion on the peptide carbonyl, and the formation of a gem-diol intermediate. The last stage involves a proton transfer from C-terminal of the substrate to the peptide nitrogen, and a cleavage of the peptide bond. The detailed GAGB-2 mechanism is described in Figure 2(B).

The support for the direct nucleophilic pathway was based on the spectroscopic detection of anhydride-type acyl-enzyme intermediates in the CPA-catalyzed hydrolysis of ester type substrates under low temperature conditions 38–41. The designation of the acyl enzyme was not confirmed by chemical trapping experiments, thereby challenging some of these results 13,40. More recently, an anhydride intermediate was detected in the CPA hydrolysis of Gly-Tyr, a slow substrate, by solid state NMR spectroscopy 42. These results seem to suggest that an anhydride intermediate could be involved in the proteolytic reaction of CPA. It was argued that the X-ray structure of a Gly-Tyr complex with CPA 43 supports this conclusion, as no water molecule is found in the active site that could interact with this dipeptide, and thus Gly-Tyr must take the anhydride path. But, Gly-Tyr was found in the complex in a conformation which is different than that expected for a regular substrate: it chelates the zinc with its peptide carbonyl (which is expected) as well as with its amino N-terminal (most probably in the neutral, deprotonated form).

This lack of a water molecule in the complex could thus be special for Gly-Tyr or maybe also for a few other slow substrates that can bind differently than normal substrates. There is also a possibility that a water molecule could get involved in the cleavage of Gly-Tyr, although it is missing from the proper position in the crystal. On the other hand, it is expected that most substrates, which are larger than Gly-Tyr, should expel a water molecule even more easily than Gly-Tyr, and subsequently could undergo an attack by Glu270 to form an anhydride. Furthermore, penetration of water molecules to the active site should

cost very little energy and thus the observation of such a molecule in the active site is not as informative as usually assumed.

Earlier isotopic studies by Breslow and Wernick were designed to follow O18 along the reaction coordinate of CPA 44›45. These studies showed that an anhydride intermediate is probably not involved in the hydrolysis of peptide substrates by CPA, and suggested that this cleavage is better rationalized by a GAGB mechanism. In the GAGB mechanism, a water molecule that is activated by Zn or by Glu270, attacks the peptide bond, looses a proton (probably to Glu270) and forms an intermediate gem-diol. Low-temperature studies from Aulds' laboratory 46 supported such suggestions. In addition, recent kinetic experiments show that it may be possible that different mechanisms operate with different substrate types: peptide hydrolysis is probably achieved via a GAGB mechanism, while ester hydrolysis could take the "anhydride" pathway 47.

As already described above, there is more than a single proposal for a GAGB pathway of CPA. Christianson and Lipscomb 13 suggested a reaction path in which the substrate binds directly to zinc while retaining the water molecule that occupies the fourth coordination site of zinc in the native structure. This water molecule may be activated by the metal ion or by Glu270 (or both), loses a proton and attacks the peptide carbonyl. The suggestion of a GAGB mechanism was based on crystallographic results of CPA complexes with transition state analog inhibitors 35›48›49 that bind to the active site in the gem-diol state. It was assumed that the two tetrahedral oxygens of the gem-diol are stabilized by their interactions with the active site. That is, the gem-diol state is highly unstable in solution, unless strong electron attractors are present near the carbonyl 50. It was concluded that the gem-diol forms only as a result of interaction with the enzyme, while none could be detected in solution with no enzyme present 50.

A significantly different GAGB mechanism was proposed by Mock 37 based on kinetic results of two diaesteriomers. The binding of the substrate enables activation of the peptide carbonyl by zinc, but the water molecule that is involved is positioned very differently. This water molecule is deprotonated by the C-terminal carboxylate of the substrate itself, adjacent to Arg127, and not by Glu270 or by the zinc ion (Fig. 2B).

Several theoretical studies have been performed in order to clarify the catalytic mechanisms of CPA and of thermolysin (TLN). Morokuma and coworkers 51 employed *ab initio* STO-3G gas phase model and suggested that the Zn-coordinated water molecule acts as a proton donor for Glu270 in CPA. They concluded that zinc plays a significant role in lowering the pK_a of its coordinated water molecule. However, gas phase calculations cannot be used to explore the issue in a quantitative way. Alex and Clark 52 constructed a simplified model of CPA and performed AM1 calculations for the different steps suggested for the water-promoted pathway proposed by Lipscomb's group 13. Alvarez-Santos et al. 53 designed a model of the active site of CPA plus substrate, containing 51 atoms and identified the water (hydroxide) attack on peptide carbonyl as the rate-determining step, with a high enthalpy barrier of 37.9 kcal/mol. This calculated activation enthalpy was dramatically decreased when a positive charge (that represented Arg127) was included. Unfortunately, such a model is not likely to reflect the proper screening of the effect of Arg127. More recently, Alvarez-Santos et al. 54 used molecular dynamics simulations and AM1 calculations on a larger model of 106 atoms, which included Arg127 (simulated by guanidinium) among other additional components. Their results show that the transition state for proton transfer from Glu270 to the peptide nitrogen is the highest peak in the full energy profile. Abashkin et al. 55 performed density functional theory calculations but had to reduce the size of the model, to a mere 26 atoms. Their results 55 suggest that the rate determining step is the formation of a tetrahedral intermediate arising from the attack of a

Zn-coordinated OH group on the carbonyl of the substrate. A semiempirical and QM/MM study of peptide hydrolysis by thermolysin was performed by Rivail 56 and co-workers while Giessner and Jacob 57 employed MNDO (with special Zn parameterization) to calculate the interactions between zinc and different ligands at the thermolysin active site. Goldblum and co-workers performed a semi-empirical QM study on the alternative mechanisms for zinc proteinases 58–60. Their results suggest that the anhydride pathway is not a viable candidate to be the mechanism of cleavage of peptides by CPA 60 and that both GAGB mechanisms are feasible 58,59. Banci et al. 61 demonstrated the mobility of Arg127 and Tyr248 and suggested 62 that both "nucleophilic" and "water-promoted" pathways are structurally feasible, although the water-promoted mechanism is favored energetically.

While the above studies have contributed to the general understanding of the mechanism of CPA, they have not provided conclusive results. Of course, one does not expect quantitative conclusions from gas phase calculations 51,52 or calculations with a fixed protein structure 53,56. Similarly, MD simulations61 that do not evaluate the chemical barriers are of limited applicability, since the availability of ground state configurations with proper water orientation does not tell us about the TS energy. Even QM/MM studies, cannot provide quantitative results without calculations of activation free energy and validation of the energetics by either using high level *ab initio* calculations of the reference reaction in water or calibration using experimental information about the reference reaction in water (see discussion in ref. 63–65. Unfortunately, these tasks have not been accomplished by the above studies.

The present study we attempts to advance the understanding of the catalytic effect of CPA in particular and metalloenzymes in general by using the empirical valence bond (EVB) method 65. In our view, at present, the EVB is the most effective tool for this purpose also *ab initio* QM/MM free energy calculations may offer additional options for studying CPA 63,66 and the same is true for semi-emprical QM/MM free energy calculations 67. The EVB evaluates the catalytic effect (the difference in activation free energy between the water and enzyme reaction) without adjusting any parameters for this purpose and does so by rigorous free energy calculations. It seems to us that only after evaluating the observed catalytic affect, we are in a position to check mechanistic hypothesis or to explore the origin of the catalytic effect. Thus we report below the results of an extensive EVB study of the mechanism of CPA and the role of the Zn^{+2} ion and key residues.

General considerations and computational methods

As described in the previous section, the proposed mechanisms for CPA may be divided to two major types: two GAGB mechanisms that results in the formation of a gem-diol intermediate and a direct nucleophilic attack that results in the formation of an anhydride intermediate. Here we decided to focus our research on GAGB mechanisms and will only provide a limited discussion of the anhydride mechanism.

The main challenge of the present work is the evaluation of the change in activation free energy, relative to the reference solution reaction, in a sufficiently reliable way to allow for a meaningful analysis of the origin of the catalytic effect. This requires very extensive sampling, which is hard to accomplish reliably by current molecular orbital QM/MM methods despite significant advances in this direction in studies of different enzymes 64. As stated above, we believe that at present the most effective strategy is to use the empirical valence bond (EVB) method (e.g. ref 8 and 65). The EVB method has been described numerous times 65,68 and has been used extensively by our group and by other research groups (e.g. refs 69–72)

In the EVB method the enzyme/substrate system is divided into “quantum” and “classical” parts. The quantum part includes the portion of the substrate and the enzyme where bonds are being broken or formed. The atoms of this part are represented by a quantum mechanical Hamiltonian and are referred to as the EVB atoms. The rest of the system is described by a classical force field. The effect of the classical part on the quantum Hamiltonian is obtained through electrostatics, van der Waals, and bonding terms. The EVB diagonal elements are given by

$$\varepsilon_i = H_{ii} = \sum_j \Delta M_j^{(i)}(b_j^{(i)}) + 1/2 \sum_m \gamma_m^i k_m^{(i)} (\theta_m^{(i)} - \theta_{0,m}^{(i)})^2 + \sum_l K_l^{(i)} \left[1 + \cos(n_l^{(i)} \phi_l^{(i)} - \delta_l^{(i)}\right] + V_{nb,rr}^i + \alpha^{(i)} + V_{nb,rs}^{(i)} + V_s \quad (1)$$

In the first equation, ΔM_j^i denotes the Morse potential relative to its minimum value for the *j*th bond in the *i*th resonance. The second and third terms, respectively, represent the bond angle bending contribution and the torsional angle twisting contribution. The variables b, θ, and φ are bond lengths, bond angles, and torsional angles, respectively. The factor γ_m^i in the second term is a coupling between bonds that are being broken or formed and those angles that depend on these bonds, and k_m is the force constant for the angle bending term. The periodicity of the potential is determined by n_l, and the variable δ is the phase shift term. The fourth term denotes nonbonded electrostatic and van der Waals interactions between the reacting groups (denoted by subscript r). The term α^i is the gas-phase energy of the *i*th state when all fragments are at infinite separation. The nonbonded interaction with the surrounding protein and solvent, denoted by subscript s, is given by $V_{nb,rs}^i$ The last term represents the internal potential energy of the protein/solvent system.

The off-diagonal elements of the Hamiltonian are represented here by a simple single exponential approximation

$$H_{ij} = A_{ij} \exp\{-\mu r\} \quad (2)$$

The r term in the H_{ij} expression is the distance between atoms whose bonding is changed upon transfer from state *i* to state *j*. The parameters A_{ij} and μ can be adjusted to reproduce the observed barrier for the reaction in solution or to reproduce gas-phase *ab initio* calculations. The actual ground-state potential surface, Eg, is obtained by diagonalizing the EVB Hamiltonian (see ref 65 for detailed discussion).

The EVB free energy is evaluated by driving the system from the reactant to the product (or intermediate) using mapping potential of the form

$$\varepsilon_m = \sum \varepsilon_i \eta_m^i \quad (3)$$

where $\eta^m = (\eta_1^m, \eta_2^m, \ldots, \eta_n^m)$ is a mapping vector whose components are changed by fixed increments during the mapping process (here, we use η rather then λ to prevent confusion with the reorganization energy). The data generated during this simulation is used to evaluate the reaction free energy, Δg(*X*), using a combination of the FEP and umbrella sampling approaches (see ref 65 for details):

$$\exp[-\beta\Delta g(X)]=\exp\left[-\beta\Delta G_{map}(\eta^0 \rightarrow \eta^m)\right]\left\langle \delta(X' - X)\exp\left[-\beta(E_g - \varepsilon_m)\right]\right\rangle_{\varepsilon_m} \quad (4)$$

where X is the reaction coordinate, $\beta = 1/k_BT$, k_B is the Bolzmann constant, η^m is the value of η that keeps the system closest to X, E_g is the ground-state energy of the EVB Hamiltonian, and $\langle\ \rangle_{\varepsilon m}$ designates an average over the trajectory with the given ε_m. $\Delta G(\eta^0 \rightarrow \eta^m)$ is the free energy associated with changing the mapping potential from ε_0 to ε_m (this ΔG is obtained by a standard FEP approach).

The reaction coordinate is taken as the difference between the values of the two mapping potentials that change during the given mapping step (e.g., $X = \varepsilon_2 - \varepsilon_1$ when we change $\eta_1$to η_2). The relevant activation barrier, $\Delta g^{\ddagger}$, is given by $\Delta g^{\ddagger} = \Delta g(X^{\ddagger}) - \Delta g(X_0)$, where X_0 and $X^{\ddagger}$ are the values of the reaction coordinate at the ground state and transition state, respectively.

The EVB/FEP/US simulations were performed with the MOLARIS simulation program73,74 using the ENZYMIX force field. Following the standard MOLARIS protocol we divided the simulation system to four regions. Region I included part of the substrate (we have used two types of substrates in our simulations: pGlu-Phe-PheOH (pGluFF) and Bz-Gly-Phe (BzGP)36) and a part of residue Glu270 (see Fig. 2 and Fig. 4). Note that because of the calibration on the water reaction, the results do not change when we include larger parts of Glu270 in the EVB region or leave these parts in the protein region. Region II included the protein plus the water molecules in and around protein up to a radius of 20 Å, and region III included protein atoms and water molecules that were subjected to distance and polarization constraints according to the surface constrained all atom solvent (SCAAS) boundary condition75. The rest of the system was represented by a bulk region with a dielectric constant of 80. The long-range electrostatic effects were treated by the local reaction field (LRF) method76 that provides one of the most rigorous ways of treating electrostatic effects in protein and other non-periodic systems. We also would like to point out that the SCAAS +LRF treatment were subjected to very extensive validation studies, in terms of the insensitivity of the calculated electrostatic free energy to changes in the size of the system ((*e.g.*, ref 77–79). We are not aware of reported studies of this type for other approaches. More considerations of the reliability of our approach are provided in the discussion section.

The Zn^{+2} ion was described by parameters 80 which were calibrated against observed structures and solvation free energies. The overall EVB parameters set is given in Table S2 of the supplement materials.

The GAGB reaction was described by considering a three-step mechanism (see Fig. 2) and four VB structures (Fig. 4) used to define the system in the EVB calculation. Note that the Zn^{+2} ion is considered as a part of the environment and not as a part of the reacting system (the consideration involved in selecting a metal ion as a part of the environment are discussed in great length in ref. 81,82). The charges of the EVB states were obtained by using Gaussian03 package 83. This was done by optimizing the structures of the EVB states in the gas phase using B3LYP/6-31+g(d) 84 and a COSMO solvation model 85 and calculating Mullikan charges for each structure. The charges used for the VB structures are given in Table S1 of the Supplementary material. The starting point of our simulation of the CPA mechanisms is a structure of CPA with pGluFF that is based on a x-ray study provided by Shoham et al.86 (CPA/pGluFF 1.46Å, R=13%). The enzyme was then subjected to 300,000 MD relaxation steps at 30K, using 0.1 fs for each step and a weak (0.03 kcal/(mol^{-1} Å $^{-2}$)) internal protein constraint (a constraint that keeps the protein atoms close to the observed X-ray structure). The mapping parameters (η)were changed in increments of 0.05

starting from the reactants (1.0,0.0,0.0,0.0) to (0.0,1.0,0.0,0.0) and then to (0.0,0.0,1.0,0.0) and finally to the products (0.0,0.0,0.0,1.0), thus driving the system from the first to the last resonance structure (see Fig. 4). We have used a simulation length of 20 ps with 1 fs stepsize at 300K for *each* of the 21 mapping steps. The first 10% of the data at each η point was discarded in the evaluation of the free energy profile. Several initial conditions were used in each case in order to ensure the stability of the results and in order to obtain a proper average over the protein configuration (leading typically to a total length of 4×440 ps). It should be noted that the convergence of the EVB simulation was examined by running longer runs and that the SCAAS +EVB calculations converge much faster than alternative methods.

The energetics from the three mapping steps were pieced together to form free energy profiles for the two mechanisms in water and in protein. We have also applied in some of our EVB calculation induced dipoles, by a polarizable force field 87. This was done to better evaluate the electrostatic effects.

One of the most crucial aspects of the EVB procedure is the parameterization of the reference reaction in water by forcing the energetics of the simulated solution reaction to reproduce the corresponding experimental (or high-level *ab initio*) results. The relevant ΔG and $\Delta g^{\ddagger}$ values used in parametrizing the solution reaction are discussed in details in the next section. The EVB simulation was first performed in water to calibrate the gas-shift, α (see eq. 1). The same value of α was used in the protein calculations. The calibration of the EVB parameters involves setting the values of α for the individual steps so the calculated ΔG would reproduce the experimental ΔG and setting the H_{ij} values for the individual steps so the calculated $\Delta g^{\ddagger}$ would reproduce the experimental $\Delta g^{\ddagger}$. The corresponding values are given in Table S2 of the Supplementary material.

The reference reaction in water was explored by including in region I the reacting substrate, the proton donor (Glu270) and the reacting water molecule. The surrounding was modeled by a SCASS water sphere whose radius was taken as 20 Å, where the resulting spherical system was surrounded by a surface of langevine dipoles which were then surrounded by a bulk system (ref. 88). The reaction for both mechanisms was simulated in the protein environment using the same protocol and the same EVB parameters as in the water simulations.

Results

A key feature of our calculation is the determination of the relevant $(\Delta G_{i->j})_{obs,w}$ and $(\Delta g^{\ddagger}{}_{i->j})_{obs,w}$ for the reference reaction in water. As a first step in such a determination, we analyzed the experimental energetics of the GAGB-1 and GAGB-2 mechanisms in water. The corresponding free energy profiles are summarized schematically in Figure 5. In the first step of the GAGB-1 mechanism in water, a proton is transferred from a water molecule to glutamic acid. The reaction free energy is given by the equation 65,89.

$$(\Delta G_1)_{obs,w}=2.3RT(pK_a[H_20]-pK_a[Glu]=15.9\ kcal/mol \quad (5)$$

,while the activation free energy is usually a few kcal/mol higher 90 and is estimated to be $(\Delta g^{\ddagger}{}_1)_{obs,w}$ ~ 18.3 kcal/mol at 297 K.

In the GAGB-2 mechanism in water, the proton is transferred from a water molecule to the C-terminal of the substrate. Using an equation similar to the one above and a pK_a value of 2.58 for the C-terminal of the substrate, the proton-transfer reaction free energy is estimated

to be $(\Delta G_1)_{obs,w}$= 13.3 kcal/mol. The activation free energy can be estimated to be $(\Delta g^{\ddagger}{}_1)_{obs,w}$ ~ 18.3 kcal/mol at 297 K 90

In the next step of the GAGB-1 and GAGB-2 mechanisms the hydroxide ion attacks the peptide carbonyl which leads to the formation of a gem-diol intermediate. The experimental free energy is estimated (based on an early systematic study 91) to be $(\Delta G_2)_{obs,w}$= 10 kcal/mol and the activation free energy is $(\Delta g^{\ddagger}{}_2)_{obs,w}$ ~ 20 kcal/mol.

In the last stage of the GAGB-1 mechanism there is a proton transfer from Glu270 to the peptide nitrogen that leads to the break of the peptide bond. Since we could not find experimental results for this reaction in water, we performed *ab initio* scans of the energy of the actual reacting system in water, using B3LYP/6-31+g(d) and a COSMO solvation model. These calculations (see Figure S3 in the Supporting Information) gave reaction free energy, $(\Delta G_3)_{obs,w}$, of about −29 ± 3 kcal/mol and an activation free energy barrier, $(\Delta g^{\ddagger}{}_3)_{obs,w}$, of about 8.5 ± 3 kcal/mol.

In the last stage of the GAGB-2 mechanism there is a proton transfer from C-terminal of the substrate to the peptide nitrogen that leads to the break of the peptide bond. As described above, we decided to gain more insight about the reaction by performing *ab initio* scans of the energy of the actual reacting system in water, using B3LYP/6-31+g(d) and a COSMO solvation model 85. These calculations (see Figure S3 in the Supporting Information) gave a free energy, $(\Delta G_3)_{obs,w}$, of about −35 ± 3 kcal/mol and an activation free energy barrier, $(\Delta g^{\ddagger}{}_3)_{obs,w}$, of about 4.8 ± 3 kcal/mol.

After analyzing the experimental results for the two mechanisms in solution, we performed EVB simulations of the two mechanisms in water, native protein and mutant protein (R127A) in different simulation conditions. The methodology of performing the calculation was already described above (see the method section). We first calibrated the energy results from the EVB simulation in water to reproduce the corresponding experimental results described above. The calibrated EVB parameters are given in Table S2 of the Supporting information. The final EVB results for the water system are summarized in Table I, where we report the calculated ΔG's and $\Delta g^{\ddagger}$ for the GAGB-1 and GAGB-2 mechanisms in different simulation conditions.

The first two simulations listed in Table I included the pGluFF substrate and did not include induced dipoles in the EVB treatment. As seen from Table I we were able to obtain a $\Delta g^{\ddagger}{}_{wat}$ of 38.8 kcal/mol for the GAGB-1 mechanism. This value is 2.9 kcal/mol above the experimentally based estimate of 35.9 kcal/mol given in Table I. For the GAGB-2 mechanism we were able to obtain a $\Delta g^{\ddagger}{}_{wat}$ of 37.3 kcal/mol, which is 4.0 kcal/mol higher than the corresponding experimentally derived estimate. Although, we could force the calculations to reproduce the experimental results in one system.

The next two simulations listed in Table I (the third and the fourth simulations) include the BzGP substrate and did not include induced dipoles. For this conditions we were able to obtain a $\Delta g^{\ddagger}{}_{wat}$ of 38.0 kcal/mol for the GAGB-1 mechanism. This value is 2.1 kcal/mol above the experimentally based estimate of 35.9 kcal/mol. For the GAGB-2 mechanism we were able to obtain a $\Delta g^{\ddagger}{}_{wat}$ of 36.9 kcal/mol, which is 3.6 kcal/mol higher than the corresponding experimentally derived estimate. In principle, we could improve this agreement with more extensive parameterization, but this would not change the conclusions obtained below.

The last two simulations listed in Table I include the BzGP substrate and used a polarizable force field. For this conditions we were able to obtain a $\Delta g^{\ddagger}{}_{wat}$ of 38.2 kcal/mol for the GAGB-1 mechanism. This value is only 2.3 kcal/mol above the experimentally based

estimate of 35.9 kcal/mol. For the GAGB-2 mechanism we were able to obtain a $\Delta g^{\ddagger}_{wat}$ of 36.7 kcal/mol, which is 3.4 kcal/mol higher than the corresponding experimentally derived estimate. In principle, we could imperious this agreement with more extensive parameters but this would not change the conclusion obtained below.

The results of the EVB simulations in the native protein are summarized in Table II. This table reports the calculated ΔG's and $\Delta g^{\ddagger}$ for the GAGB-1 and GAGB-2 mechanisms in different simulation conditions. The first two simulations listed in Table II include the pGluFF substrate and did not include induced dipoles. As seen from Table II we were able to obtain a $\Delta g^{\ddagger}_{cat}$ of 16.5 kcal/mol for the GAGB-1 mechanism. This value is only 0.5 kcal/mol above the experimentally based estimate of 14–16 kcal/mol given in Table II. For the GAGB-2 mechanism we were able to obtain a $\Delta g^{\ddagger}_{cat}$ of 20.1 kcal/mol, which is 4.1 kcal/mol higher than the corresponding experimentally derived estimate.

The next two simulations listed in Table II (the third and the fourth simulations) include the BzGP substrate and did not include induced dipoles. For this conditions we were able to obtain a $\Delta g^{\ddagger}_{cat}$ of 13.6 kcal/mol for the GAGB-1 mechanism. This value is only 2.4 kcal/mol below the experimentally based estimate of 16.0 kcal/mol. For the GAGB-2 mechanism we were able to obtain a $\Delta g^{\ddagger}_{cat}$ of 23.4 kcal/mol, which is 7.4 kcal/mol higher than the corresponding experimentally derived estimate. The calculated energetics of the GAGB-1 and GAGB-2 mechanisms in water and protein environments are depicted schematically in Figure 6. The GAGB-1 results in Figure 6 are for the third EVB simulation (BzGP/no induce dipoles) of Table I and Table II, while the GAGB-2 results are for the fourth EVB simulation (BzGP/no induce dipoles) of Table I and Table II. As seen from the comparison of the two figures we reproduced a large catalytic effect in both cases. The catalysis appears to reflect a large protein stabilization effect in both nucleophilic attack and proton transfer steps.

The last two simulations listed in Table II include the BzGP substrate and used a polarizable force field. For this model we were able to obtain a $\Delta g^{\ddagger}_{cat}$ of 13.3 kcal/mol for the GAGB-1 mechanism. This value is only 2.7 kcal/mol below the experimentally based estimate of 16.0 kcal/mol. For the GAGB-2 mechanism we were able to obtain a $\Delta g^{\ddagger}_{cat}$ of 28.9 kcal/mol, which is 12.9 kcal/mol higher than the corresponding experimentally derived estimate.

Our results for the GAGB-1 mechanism accounts for the catalytic effect regardless of the substrate size and the influence of induced dipoles. The situation becomes more problematic for the GAGB-2 mechanism where the catalytic effect is underestimated and the largest deviation is obtained for BzGP in the model with induced dipoles. More specifically the calculated $\Delta\Delta g^{\ddagger}_{w\rightarrow p}$ is around 23±2 kcal/mol in the GAGB-1 mechanism as compared to an observed effect of about 20±2 kcal/mol. On the other hand, the calculations for the GAGB-2 mechanism give $\Delta\Delta g^{\ddagger}_{w\rightarrow p}$ between 17 to 8 kcal/mol as compared to an observed value of 17±2 kcal/mol.

In a further attempt to better understand the structure/function relationship in CPA, we mutated a key residue in CPA active site to check its impact on catalysis. We mutated Arg127 to Ala127 (R127A), which based on kinetic experiments36 causes k_{cat} to decrease from 12 to 0.012. This corresponds to a 6 kcal/mol decrease in the stabilization of transition state in the rate determining step.

The results of the EVB simulation in mutant protein (R127A) are summarized in Table III. The first two simulations listed in Table III include the BzGP substrate and did not include induced dipoles. As can bee seen from the table, the trend in the results of the mutated protein for the GAGB-2 mechanism are in a disagreement with the observed mutation affect. That is, the experimental results for the GAGB-2 mechanism point to an increase in

activation energy barrier due to the mutation36, but the calculations yielded a decrease in the activation barrier in the mutant protein relative to the barrier in the native protein (see Table II and Table III). The calculated energetics of the GAGB-1 and GAGB-2 mechanisms in the native and mutant protein are depicted schematically in Figure 7. The GAGB-1 results in Figure 7 are for the third EVB simulation (BzGP/no induce dipoles) of Table II and the first EVB simulation of Table III, while the GAGB-2 results are for the fourth EVB simulation (BzGP/no induce dipoles) of Table II and the second EVB simulation of Table III.

The analysis of the results also yields the differences in $\Delta\Delta g^{\ddagger}_{cat}$ for the two mechanisms (see Table III). In the GAGB-1 mechanism the value of $\Delta\Delta g^{\ddagger}_{cat}$ is 10.6 kca/mol and 11.2 kcal/mol, respectively, for simulations without and with induced dipoles. In the GAGB-2 mechanism the value of $\Delta\Delta g^{\ddagger}_{cat}$ is −1.2 kcal/mol and −12.9 kcal/mol, respectively, for simulations with and without induced dipoles. In view of this simulated mutation effects the GAGB-2 mechanism is significantly less likely than the GAGB-1 mechanism.

The role of the metal

The presence of active site metal ion is a ubiquitous feature of enzymatic reaction, and these ions generally play a crucial role in the catalytic activity of the enzyme. In CPA, extraction of this metal atom creates an inactive enzyme, while a replacement of the zinc ion by a range of dications results in diverse activities35. Here we probed the catalytic role of the zinc ion by running EVB simulations in which we turned the zinc charge to zero. Such calculation should help in estimating the electrostatic contribution of the zinc atom to enzyme catalysis.

The results of the EVB simulation with zero charged zinc are summarized in Table IV. The first two simulations listed in Table IV include the BzGP substrate and did not include induced dipoles. As seen from Table IV we obtained a $\Delta g^{\ddagger}_{cat}$ of 35.6 kcal/mol for the GAGB-1 mechanism. This value is 0.3 kcal/mol less than the experimentally based estimate of 35.9 kcal/mol for the same reaction in water (see Table I). More importantly, this value involves a loss of 22.0 kcal/mol from the catalytic effect. For the GAGB-2 mechanism we obtained a $\Delta g^{\ddagger}_{cat}$ of 32.4 kcal/mol, which involves a loss of 9.0 kcal/mol from the catalytic effect. The last two simulations listed in Table IV include the BzGP substrate and used a polarizable force field. For this conditions we obtained a $\Delta g^{\ddagger}_{cat}$ of 28.3 kcal/mol for the GAGB-1 mechanism. This value reflects a loss of 15.0 kcal/mol from the catalytic effect. For the GAGB-2 mechanism we obtained a $\Delta g^{\ddagger}_{cat}$ of 49.7 kcal/mol, which involve a loss of 20.8 kcal/mol from the catalytic effect. Overall these calculations indicate that the electrostatic effect of the metal is by far the largest catalytic contribution in CPA and probably in other metalloenzymes8.

Direct nucleophilic attack mechanism

We have also attempted to investigate the direct nucleophilic attack mechanism (see Figure 3). In order to perform an effective EVB study of this system, it is crucial to calibrate the relevant parameters using experimental or *ab initio* information about the solution reaction. In the absence of direct experimental information we performed *ab initio* scans of the energy of the actual reacting system in water, using B3LYP/6-31+g(d) and a COSMO solvation model85 and the procedure used in 92,93. The calculations gave an activation barrier of ~50 kcal/mol, for the rate determining step of the anhydride formation. Such high energy makes this mechanism a very unlikely choice to be the correct mechanism, even with help of the protein. Thus, we decided not to perform any further calculations for this mechanism.

Discussion

The present work provided a systematic EVB study of the mechanism and catalytic effect in CPA and its mutants. Our study reproduced the observed catalytic effect in both the GAGB-1 and GAGB-2 mechanisms. But, the mutation calculations indicate that the GAGB-2 mechanism is significantly less likely than the GAGB-1 mechanism. However, our main point is not the elucidation of the exact mechanism of CPA but rather the origin of the catalytic effect in either mechanism. In this respect our main point is that the present study reproduced, for the first time, the catalytic effect in both mechanisms and found it to be largely due to the electrostatic stabilization of the substrate by the Zn^{+2} ion.

One may wonder about the reliability of our approach and about possible effect of having a radius of 20 Å on the possible effect of large protein fluctuations. However, as discussed in our recent papers 94 large scale motions do not contribute to catalysis since k_{cat} reflects the motions form ES to the TS ($ES^{\#}$) and not the binding mode. As long as k_{con} is larger than k_{cat} there is no effect of the conformational motion on catalysis. One may argue that long-range effects lead to change in catalysis. Again as demonstrated in our study of DHFR 94, we do reproduce the effect of distant mutations by our models (a task that is rarely done by other approaches) and a part of the reason for our success is the use of a stable spherical model. Here, we like to clarify that the only valid argument would be the argument that using a restricted radius of 20 Å sphere may prevent the enzyme from moving to the correct ES or $ES^{\#}$ because a part of the reorganization process is frozen. However, this problem is resolved by starting from a good initial ES structure and in some cases using larger radius in the relaxation process. In fact, the only way to explore this approximation is to verify that the resulting energetics do not change when the radius of the system increase (e.g. from 15 Å to 23 Å). This issue has been explored repeatedly in our electrostatic studies (e.g. 77–79) and has not been explored, to the best of our knowledge, in other studies. Obviously it is easy to mislead the public by implication that there are problems with the use of a finite system size, but a serious criticism should involve a validation and a demonstration of the alleged problem. This is particularly important, when there are studies that established the validity and the effectives of using a surface constrained spherical system.

At this point it is important to clarify that the Zn^{+2} stabilization effect cannot be deduced from gas phase calculations or from observation of the distance between the Zn^{+2} and the substrate. A proper evaluation must asses the screening of the field from the Zn^{+2} ion by the protein environment. When this is done, we find the enzyme loses all of its catalytic effect without the metal. It is also important to point out that in terms of active site design it is not so simple to create a binding site for the Zn^{+2} ion without screening a large part of its electrostatic field. Furthermore, the large effect obtained here of (15–22 kcal/mol) is significantly larger than the catalytic effect of the Zn^{+2} ion, for example, in carbonic anhydrase (about 11 kcal/mol)81. This means that the effect of the metal is not some constant factor, but strongly depended on the system studied.

Zinc metalloprotease constitute a part of the proteases families. These families are defined by the most critical component that is believed to be involved in catalysis. The serine proteases utilize a serine residue as the initializing nucleophile. The serine residue is part of three catalytic groups (the catalytic triad) that are essential for peptide bond hydrolysis65: Ser, His and Asp, where the serine acts as a nucleophile. Warshel et al.95 studied extensively the serine protease family using QM/MM method, to understand how the serine proteases really work. Comparing their results to ours, we find some similar trends. In both cases the rate limiting step is the creation of a tetrahedral intermediate. In the serine proteases, the ionized serine attacks the carbonyl of the substrate, forming a negatively charged intermediate (oxyanion intermediate). In zinc proteases, hydroxide ion attacks the

peptide carbonyl which leads to the formation of a tetrahedral intermediate (gem-diol intermediate). Also, their work and ours shows that the enzymes work by providing electrostatic complementarities to the change in charge distribution occurring during the reactions they catalyzed. In the zinc proteases the stabilizing affect comes mainly from the Zn^{+2} ion, in the serine proteases in comes from the charged Asp and the oxyanion hole95.

Aqvist et al.80 calculated the free energy relationship in metalloenzymes-catalyzed reaction, specifically the effects of metal ion substitution in staphylococcal nuclease (SNase). SNase is a phosphodiester-cleaving enzyme that requires a Ca^{+2} ion for its action and catalyses. The mechanism of SNase involves a general-base catalysis by Glu43, yielding a free hydroxide ion which attacks the phosphorus atom in line with the 5'-O-P ester bond. Their results showed that SNase appears to be more sensitive to ions with larger (than with smaller) hydration energies compared to Ca^{+2}, since these interact more strongly with the intermediate created OH^{-}, making the nucleophilic attack more difficult (see Figure 7 in ref. 80). The free energy relationship leading to a rate optimization are quit interesting and points toward more general features that may pertain also to other metalloenzymes. As already mentioned above the replacement of the zinc ion with a range of dications results in diverse CPA activities, with optimal activities are observed for the zinc and cobalt derivatives [30]. In CPA the alkaline-earth metals produce no activity96. Interestingly, it appears that CPA is more sensitive to replacement by transition metals with larger hydration energy than cobalt and zinc than by those with smaller hydration energies. This might be indicative of a free energy relationship similar to that found in SNase, underlying the observed optimum for Co^{+2} and Zn^{+2}.

The catalytic effect of the metal is sometimes attributed to the activation of the water molecule 35،97 or to the polarization of the carbonyl 29،35. While the traditional description is intuitively appealing, it does not have a predictive value and in fact draws attention away from the most relevant effects. That is, the real effect of the metal ion on the attacking water molecule is manifested mainly by the stabilization of the OH^{-} ion after the proton transfer step and not in destabilizing the neutral water molecule. The same is also true with regards to the polarization of the carbonyl. That is, the metal catalyzes the reaction by stabilizing the $C\text{-}O^{-}$ oxyanion system and not by changing the charge distribution of the C=O system in the ground state. In fact looking on the $C\text{-}O^{-}\text{---}Zn^{+2}$ interaction provide much more powerful way of assessing the TS stabilization than estimates of the polarization of C=O bond 8.

The idea that enzymes accelerate their reaction by entropic effects has played a major role in many proposals about the origin of enzyme catalysis, including the action of metalloenzymes. This idea implies that binding to an enzyme active site freezes the motion of the reaction fragments and eliminates their entropic contribution $\Delta S^{\ddagger}_{w}$), to the activation energy. In fact, several works 28،35،98 invoked the effect of orientating the attacking water as a major catalytic effect. Thus, one may wonder whether entropic effects play a role in CPA catalysis. Although this is an appealing idea, we do not believe that entropic effects play here a major part. This view was established in detailed studies of related cases, such as the reaction of serine proteases 99 and other systems 100. Studies of this proposal in CPA are left to subsequent works.

Conclusion

Overall, we believe that the present work provided what is perhaps the most quantitative study of the catalytic effect in CPA. Here the issue is not so much the actual GAGB mechanism, but the nature of the origin of the catalytic power. It is found that the TS stabilization is mainly due to the electrostatic effect of the Zn^{+2} ion in its specific environment. This is probably the origin of the catalytic effect in similar zinc enzymes.

Supplementary Material

Refer to Web version on PubMed Central for supplementary material.

Acknowledgments

This work was supported by NIH grant GM24492.We gratefully acknowledge the University of Southern California's High Performance Computing and Communications Center for computer time.

This work was supported by Grant GM24492 from the National Institutes of Health (NIH).

REFERENCES

1. Ellis WR. Metalloenzymes. Encyclopedia of Molecular Cell Biology and Molecular Medicine. 2006
2. Martini D, Ranieri-Raggi M, Sabbatini ARM, Moir AJG, Polizzi E, Mangani S, Raggi A. Characterization of the metallocenter of rabbit skeletal muscle AMP deaminase. A new model for substrate interactions at a dinuclear cocatalytic Zn site. Biochimica Et Biophysica Acta-Proteins And Proteomics. 2007; 1774:1508–1518.
3. Nowotny M, Gaidamakov SA, Crouch RJ, Yang W. Crystal structures of RNase H bound to an RNA/DNA hybrid: Substrate specificity and metal-dependent catalysis. Cell. 2005; 121(7):1005–1016. [PubMed: 15989951]
4. Holm RH, Kennepohl P, Solomon EI. Structural and functional aspects of metal sites in biology. Chemical Reviews. 1996; 96(7):2239–2314. [PubMed: 11848828]
5. Steitz TA, Smerdon SJ, Jager J, Joyce CM. A Unified Polymerase Mechanism For Nonhomologous Dna And Rna-Polymerases. Science. 1994; 266(5193):2022–2025. [PubMed: 7528445]
6. Aqvist J, Fothergill M, Warshel A. Computer-Simulation Of The Co2/Hco3-Interconversion Step In Human Carbonic Anhydrase-I. Journal Of The American Chemical Society. 1993; 115(2):631–635.
7. Oelschlaeger P, Klahn M, Beard WA, Wilson SH, Warshel A. Magnesium-cationic dummy atom molecules enhance representation of DNA polymerase beta in molecular dynamics simulations: Improved accuracy in studies of structural features and mutational effects. Journal Of Molecular Biology. 2007; 366(2):687–701. [PubMed: 17174326]
8. Warshel A, Sharma PK, Kato M, Xiang Y, Liu H, Olsson MHM. Electrostatic Basis for Enzyme Catalysis. Chemical Reviews. 2006; 106(8):3210–3235. [PubMed: 16895325]
9. Lee TS, Lopez CS, Giambasu GM, Martick M, Scott WG, York DM. Role of Mg2+ in hammerhead ribozyme catalysis from molecular simulation. Journal Of The American Chemical Society. 2008; 130(10):3053–3064. [PubMed: 18271579]
10. Wu XH, Quan JM, Wu YD. Theoretical study of the catalytic mechanism and metal-ion dependence of peptide deformylase. Journal Of Physical Chemistry B. 2007; 111(22):6236–6244.
11. Waldschmidt-Leitz E, Purr A. Berichte. 1929; 62B:2217–2226.
12. Anson ML. J Gen Physiol. 1937; 20:663–669. [PubMed: 19873019]
13. Christianson DW, Lipscomb WN. Carboxypeptidase-A. Accounts Of Chemical Research. 1989; 22(2):62–69.
14. Vallee BL, Galdes A. The Metallobiochemistry Of Zinc Enzymes. Advances In Enzymology And Related Areas Of Molecular Biology. 1984; 56:283–430. [PubMed: 6364704]
15. Ondetti MA, Cushman DW. Enzymes Of The Renin-Angiotensin System And Their Inhibitors. Annual Review Of Biochemistry. 1982; 51:283–308.
16. Ondetti MA, Cushman DW. Design Of Specific Inhibitors Of Angiotensin-Converting Enzyme - New Class Of Orally Active Antihypertensive Agents. Science. 1977; 196(4288):441–444. [PubMed: 191908]
17. Malfroy B, Swerts JP, Guyon A, Roques BP, Schwartz JC. High-Affinity Enkephalin-Degrading Peptidase In Brain Is Increased After Morphine. Nature. 1978; 276(5687):523–526. [PubMed: 214708]

18. Duffy MJ, Maguire TM, Hill A, McDermott E, O'Higgins N. Metalloproteinases: role in breast carcinogenesis, invasion and metastasis. Breast Cancer Research. 2000; 2(4):252–257. [PubMed: 11250717]
19. Hemmings FJ, Farhan M, Rowland J, Banken L, Jain R. Tolerability and pharmacokinetics of the collagenase-selective inhibitor Trocade (TM) in patients with rheumatoid arthritis. Rheumatology. 2001; 40(5):537–543. [PubMed: 11371662]
20. Witty JP, Foster SA, Stricklin GP, Matrisian LM, Stern PH. Parathyroid hormone-induced resorption in fetal rat limb bones is associated with production of the metalloproteinases collagenase and gelatinase B. Journal Of Bone And Mineral Research. 1996; 11(1):72–78. [PubMed: 8770699]
21. Woessner JF. The Family Of Matrix Metalloproteinases. Inhibition Of Matrix Metalloproteinases: Therapeutic Potential. 1994; 732:11–21.
22. Celentano DC, Frishman WH. Matrix metalloproteinases and coronary artery disease: A novel therapeutic target. Journal Of Clinical Pharmacology. 1997; 37(11):991–1000. [PubMed: 9505991]
23. Paul R, Lorenzl S, Koedel U, Sporer B, Vogel U, Frosch M, Pfister HW. Matrix metalloproteinases contribute to the blood-brain barrier disruption during bacterial meningitis. Annals Of Neurology. 1998; 44(4):592–600. [PubMed: 9778257]
24. White AD, Bocan TMA, Boxer PA, Peterson JT, Schrier D. Emerging therapeutic advances for the generation matrix metalloproteinase inhibitors. Current Pharmaceutical Design. 1997; 3(1):45–58.
25. Ebata M, Fukuda Y, Nakano I, Katano Y, Fujimoto N, Hayakawa T. Serum levels of tissue inhibitor of metalloproteinases-2 and of precursor form of matrix metalloproteinase-2 in patients with liver disease. Liver. 1997; 17(6):293–299. [PubMed: 9455735]
26. Vallee BL, Auld DS. Zinc - Biological Functions And Coordination Motifs. Accounts Of Chemical Research. 1993; 26(10):543–551.
27. Vendrell J, Querol E, Aviles FX. Metallocarboxypeptidases and their protein inhibitors - Structure, function and biomedical properties. Biochimica Et Biophysica Acta-Protein Structure And Molecular Enzymology. 2000; 1477(1–2):284–298.
28. Matthews BW. Structural Basis Of The Action Of Thermolysin And Related Zinc Peptidases. Accounts Of Chemical Research. 1988; 21(9):333–340.
29. Lipscomb WN. Carboxypeptidase-A Mechanisms. Proceedings Of The National Academy Of Sciences Of The United States Of America-Biological Sciences. 1980; 77(7):3875–3878.
30. Patchett AA, Cordes EH. The design and properties of N-carboxyalkyldipeptide inhibitors of angiotensin converting enzyme. Adv Enzymol. 1985; 57:1–84. [PubMed: 2994404]
31. Martin MT, Holmquist B, Riordan JF. An Angiotensin Converting Enzyme-Inhibitor Is A Tight-Binding Slow Substrate Of Carboxypeptidase-A. Journal Of Inorganic Biochemistry. 1989; 36(1): 39–50. [PubMed: 2746220]
32. Rees DC, Lewis M, Lipscomb WN. Refined Crystal-Structure Of Carboxypeptidase-A At 1.54 A Resolution. Journal Of Molecular Biology. 1983; 168(2):367–387. [PubMed: 6887246]
33. Greenblatt HM, Feinberg H, Tucker PA, Shoham G. Carboxypeptidase A: Native, zinc-removed and mercury-replaced forms. Acta Crystallographica Section D-Biological Crystallography. 1998; 54:289–305.
34. Kilshtain-Vardi A, Glick M, Greenblatt HM, Goldblum A, Shoham G. Refined structure of bovine carboxypeptidase A at 1.25 angstrom resolution. Acta Crystallographica Section D-Biological Crystallography. 2003; 59:323–333.
35. Feinberg H, Greenblatt HM, Shoham G. Structural Studies Of The Role Of The Active-Site Metal In Metalloenzymes. Journal Of Chemical Information And Computer Sciences. 1993; 33(3):501–516. [PubMed: 8320293]
36. Phillips MA, Fletterick R, Rutter WJ. Arginine-127 Stabilizes The Transition-State In Carboxypeptidase. Journal Of Biological Chemistry. 1990; 265(33):20692–20698. [PubMed: 2243116]
37. Mock WL, Zhang JZ. Mechanistically Significant Diastereoselection In The Sulfoximine Inhibition Of Carboxypeptidase-A. Journal Of Biological Chemistry. 1991; 266(10):6393–6400. [PubMed: 2007591]

38. Makinen MW, Kuo LC, Dymowski JJ, Jaffer S. Catalytic Role Of The Metal-Ion Of Carboxypeptidase-A In Ester Hydrolysis. Journal Of Biological Chemistry. 1979; 254(2):356–366. [PubMed: 33168]
39. Suh JH, Park TH, Hwang BK. Comparable Rates For Cleavage Of Amide And Ester Bonds Through Nucleophilic-Attack By Carboxylate Anion And General Acid Catalysis By Metal-Bound Water In A Carboxypeptidase-A Model. Journal Of The American Chemical Society. 1992; 114(13):5141–5146.
40. Sander ME, Witzel H. Direct Chemical Evidence For The Mixed Anhydride Intermediate Of Carboxypeptidase A In Ester And Peptide Hydrolysis. Biochemical And Biophysical Research Communications. 1985; 132(2):681–687. [PubMed: 4062944]
41. Mustafi D, Makinen MW. Catalytic Conformation Of Carboxypeptidase-A -Structure Of A True Enzyme Reaction Intermediate Determined By Electron-Nuclear Double-Resonance. Journal Of Biological Chemistry. 1994; 269(6):4587–4595. [PubMed: 8308030]
42. Lee HC, Ko YH, Bin Baek S, Kim DH. Detection of an anhydride intermediate in the carboxypeptidase a catalyzed hydrolysis of a peptide substrate by solid state NMR spectroscopy and its mechanistic implication. Bioorganic & Medicinal Chemistry Letters. 1998; 8(23):3379–3384. [PubMed: 9873738]
43. Christianson DW, Lipscomb WN. X-Ray Crystallographic Investigation Of Substrate Binding To Carboxypeptidase-A At Subzero Temperature. Proceedings Of The National Academy Of Sciences Of The United States Of America. 1986; 83(20):7568–7572. [PubMed: 3463986]
44. Breslow R, Wernick DL. Unified Picture Of Mechanisms Of Catalysis By Carboxypeptidase. Proceedings Of The National Academy Of Sciences Of The United States Of America. 1977; 74(4):1303–1307. [PubMed: 266172]
45. Breslow R, Wernick D. Mechanism Of Catalysis By Carboxypeptidase-A. Journal Of The American Chemical Society. 1976; 98(1):259–261. [PubMed: 1244372]
46. Auld DS, Galdes A, Geoghegan KF, Holmquist B, Martinelli RA, Vallee BL. Cryospectrokinetic Characterization Of Intermediates In Biochemical Reactions -Carboxypeptidase-A. Proceedings Of The National Academy Of Sciences Of The United States Of America-Biological Sciences. 1984; 81(16):5041–5045.
47. Lee M, Kim DH. Hippuryl-alpha-methylphenylalanine and Hippuryl-alpha-methylphenyllactic acid as substrates for carboxypeptidase A. Syntheses, kinetic evaluation and mechanistic implication. Bioorganic & Medicinal Chemistry. 2000; 8(4):815–823. [PubMed: 10819170]
48. Christianson DW, Lipscomb WN. Comparison Of Carboxypeptidase-A And Thermolysin - Inhibition By Phosphonamidates. Journal Of The American Chemical Society. 1988; 110(16): 5560–5565.
49. Christianson DW, Lipscomb WN. Structure Of The Complex Between An Unexpectedly Hydrolyzed Phosphonamidate Inhibitor And Carboxypeptidase-A. Journal Of The American Chemical Society. 1986; 108(3):545–546.
50. Shoham G, Christianson DW, Oren DA. Complex Between Carboxypeptidase-A And A Hydrated Ketomethylene Substrate-Analog. Proceedings Of The National Academy Of Sciences Of The United States Of America. 1988; 85(3):684–688. [PubMed: 3422451]
51. Nakagawa S, Umeyama H, Kitaura K, Morokuma K. A Molecular-Orbital Study On The Zinc-Water-Glu 270 System In Carboxypeptidase-A. Chemical & Pharmaceutical Bulletin. 1981; 29(1): 1–6.
52. Alex A, Clark T. Mo-Studies Of Enzyme Reaction-Mechanisms.1. Model Molecular-Orbital Study Of The Cleavage Of Peptides By Carboxypeptidase-A. Journal Of Computational Chemistry. 1992; 13(6):704–717.
53. Alvarezsantos S, Gonzalezlafont A, Lluch JM, Oliva B, Aviles FX. On The Water-Promoted Mechanism Of Peptide Cleavage By Carboxypeptidase-A - A Theoretical-Study. Canadian Journal Of Chemistry-Revue Canadienne De Chimie. 1994; 72(10):2077–2083.
54. Alvarez-Santos S, Gonzalez-Lafont A, Lluch JM, Oliva B, Aviles FX. Theoretical study of the role of arginine 127 in the water-promoted mechanism of peptide cleavage by carboxypeptidase A. New Journal Of Chemistry. 1998; 22(4):319–325.

55. Abashkin, YG.; Burt, SK.; Collins, JR.; Cachau, RE.; Russo, RN.; Erickson, JW. Metal-L igand Interactions. Russo, RN.; Salahub, DR., editors. Kluwer, Dordrecht; 1996. p. 1-22.
56. Antonczak S, Monard G, Ruiz-Lopez MF, Rivail JL. A semiempirical and QM/MM study. Modeling of peptide hydrolysis by thermolysin. Journal Of The American Chemical Society. 1998; 120(34):8825–8833.
57. Giessnerprettre C, Jacob O. A Theoretical-Study Of Zn++ Interacting With Models Of Ligands Present At The Thermolysin Active-Site. Journal Of Computer-Aided Molecular Design. 1989; 3(1):23–37. [PubMed: 2715793]
58. Kilshtain-Vardi A, Shoham G, Goldblum A. Mechanism of action of zinc proteinases: A MNDO/d/H study of alternative general-acid general-base catalytic pathways for carboxypeptidase-A. International Journal Of Quantum Chemistry. 2002; 88(1):87–98.
59. Kilshtain-Vardi A, Shoham G, Goldblum A. Theoretical studies of catalysis by carboxypeptidase A: Could gas-phase calculations support a mechanism? Collection Of Czechoslovak Chemical Communications. 2003; 68(11):2055–2079.
60. Vardi-Kilshtain A, Shoham G, Goldblum A. Anhydride formation is not a valid mechanism for peptide cleavage by carboxypeptidase-A: a semiempirical reaction pathway study. Molecular Physics. 2003; 101(17):2715–2724.
61. Banci L, Schroder S, Kollman PA. Molecular-Dynamics Characterization Of The Active Cavity Of Carboxypeptidase-A And Some Of Its Inhibitor Adducts. Proteins-Structure Function And Genetics. 1992; 13(4):288–305.
62. Banci L, Carloni P, Orioli PL. Molecular-Dynamics Studies On Mutants Of Cu,Zn Superoxide-Dismutase - The Functional-Role Of Charged Residues In The Electrostatic Loop-Vii. Proteins-Structure Function And Genetics. 1994; 18(3):216–230.
63. Rosta E, Klahn M, Warshel A. Towards Accurate Ab Initio QM/MM Calculations of Free-Energy Profiles of Enzymatic Reactions. J Phys Chem B. 2006; 110(6):2934–2941. [PubMed: 16471904]
64. Shurki A, Warshel A. Structure/function correlations of proteins using MM, QM/MM, and related approaches: Methods, concepts, pitfalls, and current progress. Adv Protein Chem. 2003; 66:249–313. [PubMed: 14631821]
65. Warshel, A. Computer Modeling of Chemical Reactions in Enzymes and Solutions. New York: John Wiley & Sons; 1991.
66. Mulholland AJ. Modelling enzyme reaction mechanisms, specificity and catalysis. Drug Discovery Today. 2005; 10(20):1393–1402. [PubMed: 16253878]
67. Truhlar DG, Gao JL, Garcia-Viloca M, Alhambra C, Corchado J, Sanchez ML, Poulsen TD. Ensemble-averaged variational transition state theory with optimized multidimensional tunneling for enzyme kinetics and other condensed-phase reactions. International Journal of Quantum Chemistry. 2004; 100(6):1136–1152.
68. Kamerlin SCL, Haranczyk M, Warshel A. Progress in Ab Initio QM/MM Free-Energy Simulations of Electrostatic Energies in Proteins: Accelerated QM/MM Studies of pK(a), Redox Reactions and Solvation Free Energies. Journal Of Physical Chemistry B. 2009; 113(5):1253–1272.
69. Kim Y, Corchado JC, Villa J, Xing J, Truhlar DG. Multiconfiguration molecular mechanics algorithm for potential energy surfaces of chemical reactions. Journal Of Chemical Physics. 2000; 112(6):2718–2735.
70. Schmitt UW, Voth GA. Multistate empirical valence bond model for proton transport in water. Journal Of Physical Chemistry B. 1998; 102(29):5547–5551.
71. Vuilleumier R, Borgis D. An extended empirical valence bond model for describing proton transfer in H+(H2O)(n) clusters and liquid water. Chemical Physics Letters. 1998; 284(1–2):71–77.
72. Warshel, A.; Florian, J. The empirical valence bond (EVB) method. In: Schreiner, PR., editor. The Encyclopedia of Computational Chemistry. Chichester, UK: John Wiley & Sons; 2004.
73. Lee FS, Chu ZT, Warshel A. Microscopic And Semimicroscopic Calculations Of Electrostatic Energies In Proteins By The Polaris And Enzymix Programs. J Comput Chem. 1993; 14(2):161–185.
74. Chu, ZT.; Villà, J.; Strajbl, M.; Schutz, CN.; Shurki, A.; Warshel, A. MOLARIS Version beta 9.05. beta 9.05. Los Angeles: 2004.

75. King G, Warshel A. A Surface Constrained All-Atom Solvent Model For Effective Simulations Of Polar Solutions. J Chem Phys. 1989; 91(6):3647–3661.
76. Lee FS, Warshel A. A Local Reaction Field Method for Fast Evaluation of Long-Range Electrostatic Interactions in Molecular Simulations. J Chem Phys. 1992; 97(5):3100–3107.
77. Alden RG, Parson WW, Chu ZT, Warshel A. Calculations of Electrostatic Energies in Photosynthetic Reaction Centers. J Am Chem Soc. 1995; 117(49):12284–12298.
78. Sham YY, Warshel A. The surface constraint all atom model provides size independent results in calculations of hydration free energies. J Chem Phys. 1998; 109(18):7940–7944.
79. Warshel A, Sharma PK, Kato M, Parson WW. Modeling electrostatic effects in proteins. Biochimica et Biophysica Acta (BBA) - Proteins & Proteomics. 2006; 1764(11):1647.
80. Åqvist J, Warshel A. Free Energy Relationships in Metalloenzyme-Catalyzed Reactions. Calculations of the Effects of Metal Ion Substitutions in Staphylococcal Nuclease. J Am Chem Soc. 1990; 112:2860–2868.
81. Åqvist J, Warshel A. Computer Simulation of the Initial Proton Transfer Step in Human Carbonic Anhydrase I. J Mol Biol. 1992; 224:7–14. [PubMed: 1312606]
82. Aqvist J, Warshel A. Simulation of Enzyme Reactions Using Valence Bond Force Fields and Other Hybrid Quantum/Classical Approaches. Chem Rev. 1993; 93:2523–2544.
83. Frisch MJ, Trucks GW, Schlegel HB, Scuseria GE, Robb MA, Cheeseman JR, Montgomery JA, Vreven JT, Kudin KN, Burant JC, Millam JM, Iyengar SS, Tomasi J, V. Barone BM, Cossi M, Scalmani G, Rega N, G. A. Petersson HN, Hada M, Ehara M, Toyota K, R. Fukuda JH, Ishida M, Nakajima T, Honda Y, Kitao O, H. Nakai MK, Li X, Knox JE, Hratchian HP, Cross JB, C. Adamo JJ, Gomperts R, Stratmann RE, Yazyev O, A. J. Austin RC, Pomelli C, Ochterski JW, Ayala PY, K. Morokuma GAV, Salvador P, Dannenberg JJ, V. G. Zakrzewski SD, Daniels AD, Strain MC, O. Farkas DKM, Rabuck AD, Raghavachari K, J. B. Foresman JVO, Cui Q, Baboul AG, Clifford S, J. Cioslowski BBS, Liu G, Liashenko A, Piskorz P, I. Komaromi RLM, Fox DJ, Keith T, Al-Laham MA, C.Y. Peng AN, Challacombe M, Gill PMW, B. Johnson WC, Wong MW, Gonzalez C, Pople JA. 2004 Gaussian 03, Revision C.03.
84. Hehre WJ, Ditchfie R, Pople JA. Self-Consistent Molecular-Orbital Methods.12. Further Extensions Of Gaussian-Type Basis Sets For Use In Molecular-Orbital Studies Of Organic-Molecules. Journal Of Chemical Physics. 1972; 56(5) 2257-&.
85. Klamt A, Schuurmann G. Cosmo - A New Approach To Dielectric Screening In Solvents With Explicit Expressions For The Screening Energy And Its Gradient. Journal Of The Chemical Society-Perkin Transactions 2. 1993; (5):799–805.
86. Kilshtain-Vardi A, Shoham G. Unpublished results.
87. Warshel A, Kato M, Pisliakov AV. Polarizable force fields: History, test cases, and prospects. Journal Of Chemical Theory And Computation. 2007; 3:2034–2045.
88. Lee FS, Chu ZT, Warshel A. Microscopic and Semimicroscopic Calculations of Electrostatic Energies in Proteins by the POLARIS and ENZYMIX Programs. J Comp Chem. 1993; 14:161–185.
89. Aqvist J, Warshel A. Calculations of Free Energy Profiles for the Staphylococcal Nuclease Catalyzed Reaction. Biochemistry. 1989; 28:4680–4689. [PubMed: 2765507]
90. Åqvist J, Warshel A. Calculations of Free Energy Profiles for the Staphylococcal Nuclease Catalyzed Reaction. Biochemistry. 1989; 28:4680–4689. [PubMed: 2765507]
91. Štrajbl M, Florián J, Warshel A. Ab Initio Evaluation of the Potential Surface for General Base-Catalyzed Methanolysis of Formamide: A Reference Solution Reaction for Studies of Serine Proteases. J Am Chem Soc. 2000; 122(22):5354–5366.
92. Kamerlin SCL, Florian J, Warshel A. Associative versus dissociative mechanisms of phosphate monoester hydrolysis: On the interpretation of activation entropies. Chemphyschem. 2008; 9(12): 1767–1773. [PubMed: 18666265]
93. Kamerlin SCL, Williams NH, Warshel A. Dineopentyl phosphate hydrolysis: Evidence for stepwise water attack. Journal Of Organic Chemistry. 2008; 73(18):6960–6969. [PubMed: 18729515]
94. Liu H, Warshel A. The Catalytic Effect of Dihydrofolate Reductase and Its Mutants Is Determined by Reorganization Energies. Biochemistry. 2007; 46:6011–6025. [PubMed: 17469852]

95. Warshel A, Naray-Szabo G, Sussman F, Hwang J-K. How do Serine Proteases Really Work? Biochemistry. 1989; 28:3629–3637. [PubMed: 2665806]

96. Vallee, BL.; Galdes, A.; Auld, DS.; Riordan, JF. Spiro, TG., editor. New York: Wiley; 1983. p. 25-75.

97. Lipscomb WN. Structure And Catalysis Of Enzymes. Annual Review Of Biochemistry. 1983; 52:17–34.

98. Lipscomb WN. Acceleration Of Reactions By Enzymes. Accounts Of Chemical Research. 1982; 15(8):232–238.

99. Villà J, Štrajbl M, Glennon TM, Sham YY, Chu ZT, Warshel A. How Important are Entropy Contributions in Enzymatic Catalysis? Proc Natl Acad Sci USA. 2000; 97:11899–11904. [PubMed: 11050223]

100. Sharma PK, Xiang Y, Kato M, Warshel A. What Are the Roles of Substrate-Assisted Catalysis and Proximity Effects in Peptide Bond Formation by the Ribosome? Biochemistry. 2005; 44(34): 11307–11314. [PubMed: 16114867]

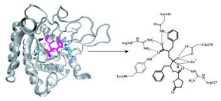

Figure 1.
The structure of CPA with a transition state analogue pGluFF. The active site zinc cation (green sphere), pGluFF (magenta) and several key residues (stick representation) are shown in more details. Schematic description of the CPA active site, depicting key residues that are involved in the binding of the transition state analogue pGluFF (bold) are shown in the inset.

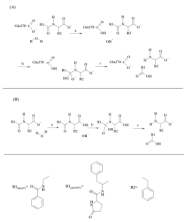

Figure 2.

A schematic description of the proposed General-Acid-General-Base (GAGB) reaction mechanisms

(A) The GAGB-1 mechanism: In the first step, A, a proton is transferred from a water molecule to glutamic acid. In the second step, B, the OH^- ion attacks the peptide carbonyl which leads to the formation of a gem-diol intermediate. In the last step, C, a proton is transferred from Glu270 to the peptide nitrogen that leads to the cleavage of the peptide bond.

(B) The GAGB-2 mechanism: In the first step, A, a proton is transferred from a water molecule to the C-terminal of the substrate. In the second step, B, the OH^- ion attacks the peptide carbonyl which leads to the formation of a gem-diol intermediate. In the last step, C, a proton is transferred from the C-terminal of the substrate to the peptide nitrogen that leads to the cleavage of the peptide bond.

The structures of R1 and R2 in pGluFF and BzGP substrates are given in the lower part of the figure.

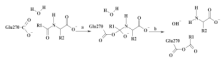

Figure 3.
A schematic description of the direct nucleophilic attack mechanism: In the first step, A, Glu270 attacks the carbonyl which leads to the formation anhydride intermediate. In the next step, B, a proton is transferred from a water molecule to the peptide nitrogen that leads to the cleavage of the peptide bond. The structure of R1 and R2 are shown in Figure 2.

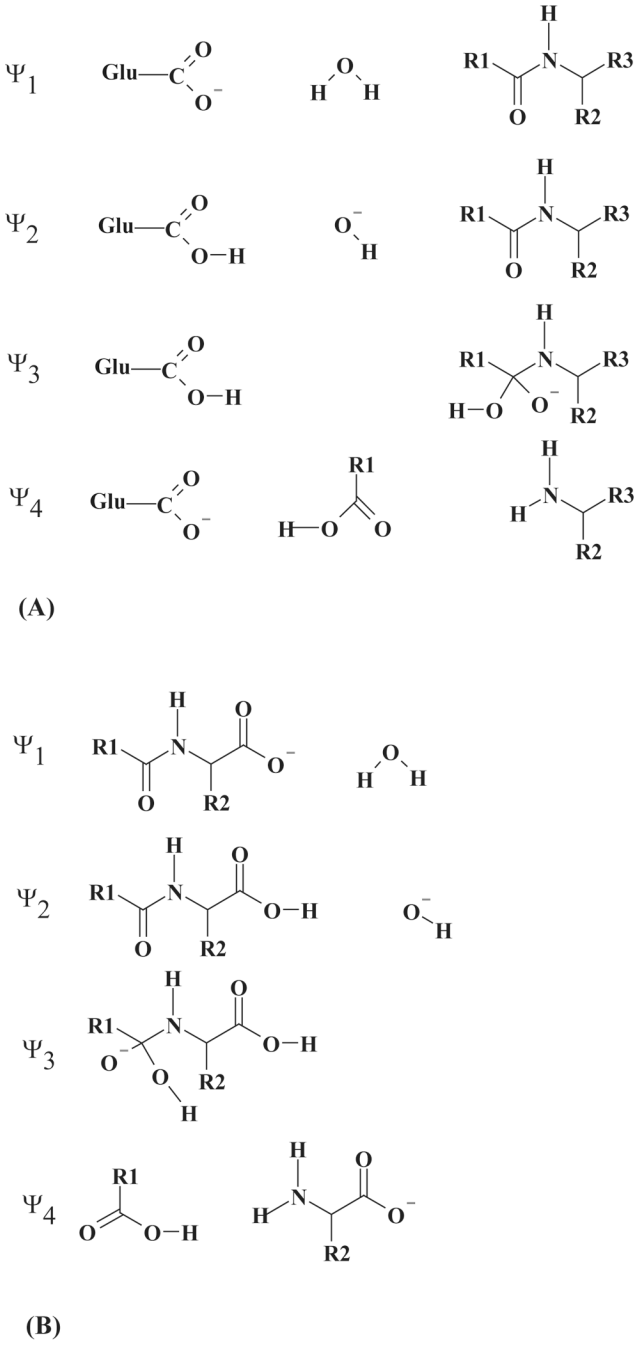

Figure 4.
The four VB structures used to describe the CPA reaction: (A) GAGB-1 mechanism. (B) GAGB-2 mechanism. Note that the Zn^{+2} ion is not a part of EVB region.

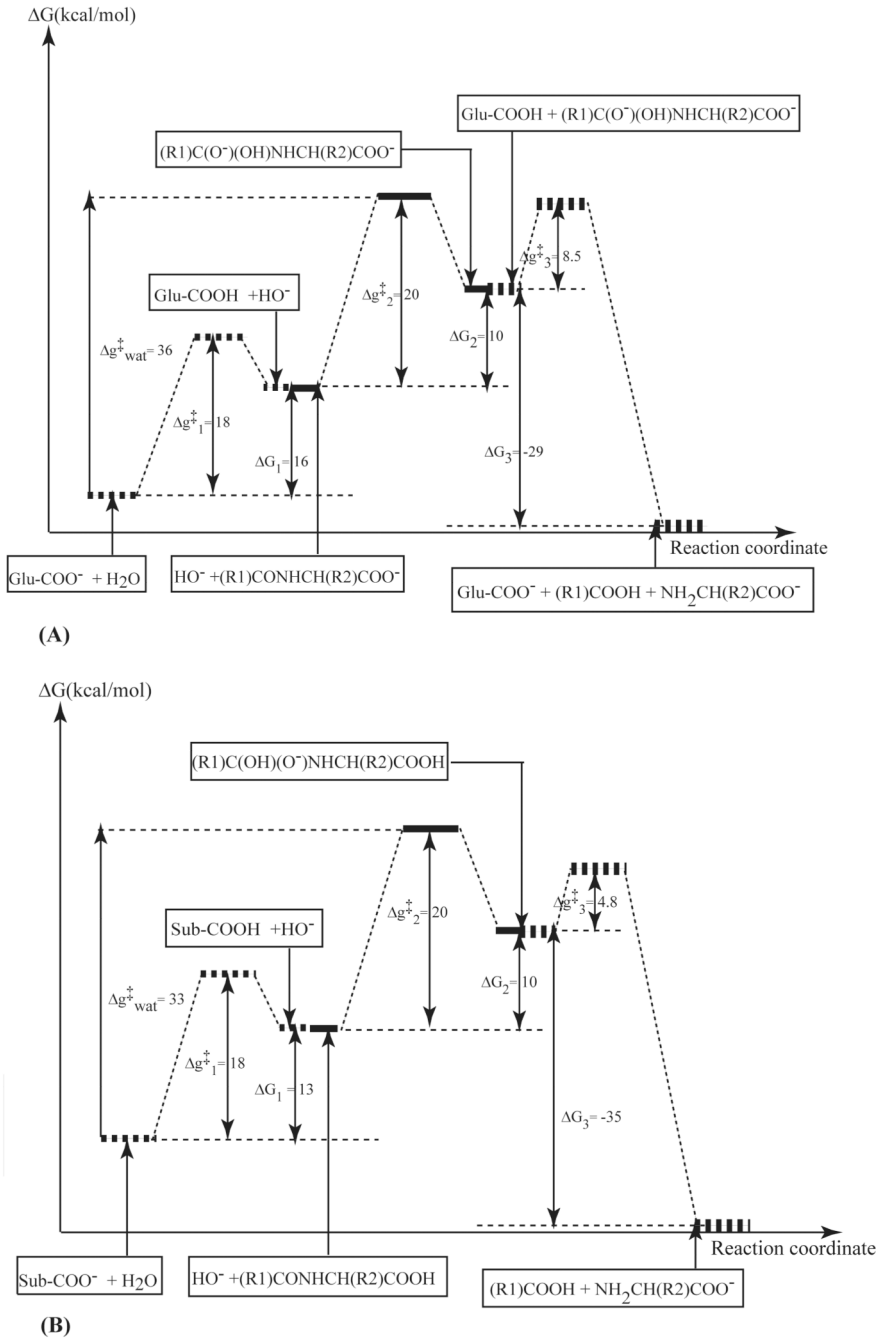

Figure 5.

Free energy diagram, based on interpolating relevant experimental data (see text), for the reference solution reactions corresponding to the mechanisms proposed for CPA. (A) and (B) describe the GAGB-1 and GAGB-2 mechanisms, respectively. The structures of R1 and R2 are given in Figure 2.

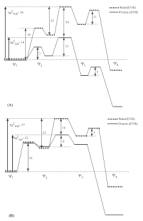

Figure 6.
Schematic description of the EVB/FEP free energy profiles in water and in CPA for the GAGB-1 (A) and GAGB-2 (B) mechanisms. The Roman numerals refer to the valence bond structures of Figure 4. Energies are in kcal/mol. The profiles are based on data given in Table I and Table II.

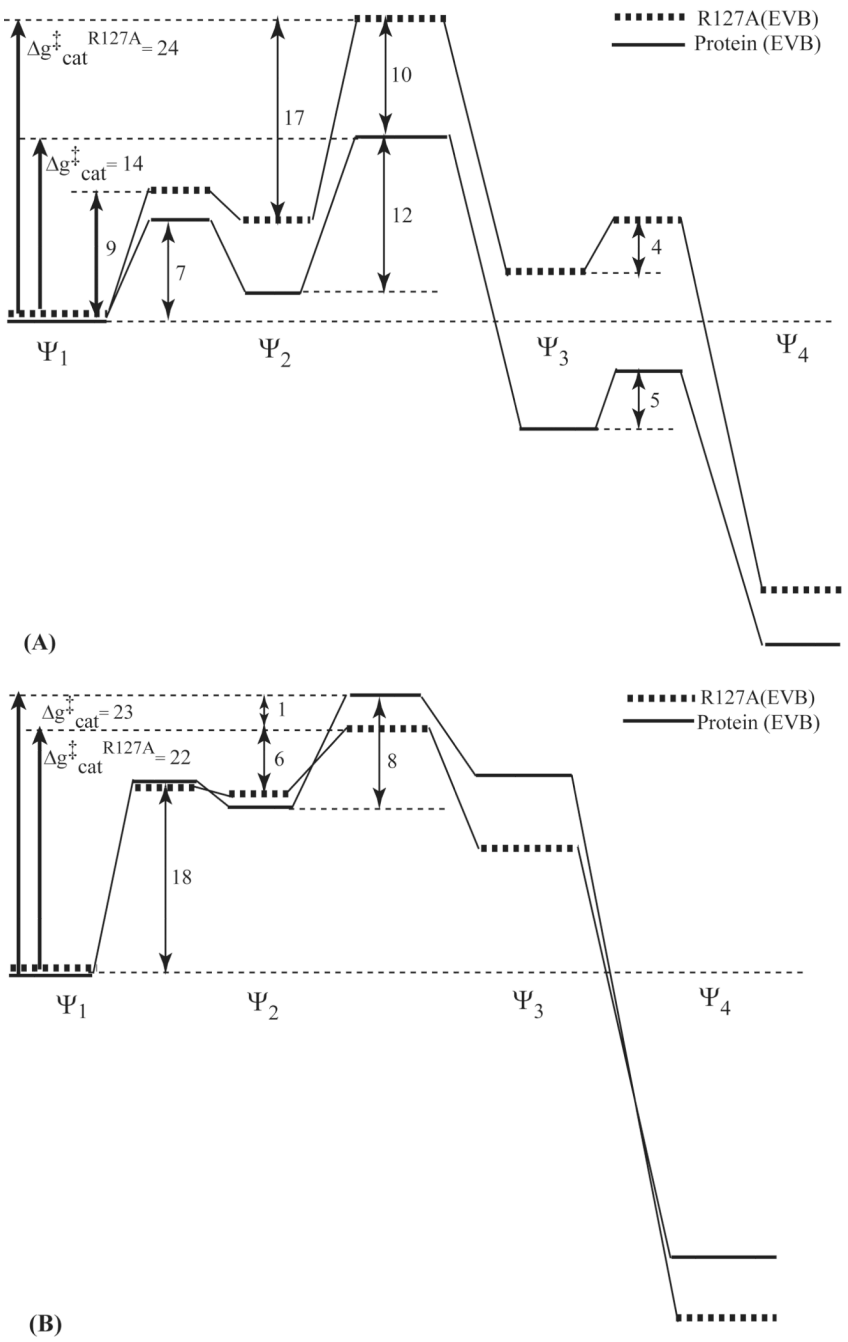

Figure 7.

Schematic description of the EVB/FEP free energy profiles in native CPA and mutant CPA (R127A) for the GAGB-1 (A) and GAGB-2 (B) mechanisms. The Roman numerals refer to the valence bond structures of Figure 4. Energies are in kcal/mol. The profiles are based on the data given in Table II and Table III.

Table 1

EVB reaction free energies and activation free energies for the reference reaction in water [a].

	$\Delta g^{\ddagger}_1$	ΔG_1	$\Delta g^{\ddagger}_2$	ΔG_2	$\Delta g^{\ddagger}_3$	ΔG_3	$\Delta g^{\ddagger}_{wat}$
Water(pGluFF) GAGB-1	18.3(18.3)	15.4(15.9)	23.4(20.0)	10.7(10.0)	12.4(8.5)	−30.0(−29.0)	38.8(35.9)
Water(pGluFF) GAGB-2	23.4(18.3)	14.9(13.3)	22.4(20.0)	9.3(10.0)	5.2(4.8)	−36.2(−35.0)	37.3(33.3)
Water(BzGP) GAGB-1	19.3(18.3)	15.3(15.9)	22.7(20.0)	9.9(10.0)	10.8(8.5)	−32.5(−29.0)	38.0(35.9)
Water(BzGP) GAGB-2	18.4(18.3)	13.6(13.3)	23.3(20.0)	9.0(10.0)	5.2(4.8)	−36.2(−35.0)	36.9(33.3)
Water(BzGP) GAGB-1 (induce)	19.9(18.3)	15.4(15.9)	22.8(20.0)	11.4(10.0)	10.7(8.5)	−30.3(−29.0)	38.2(35.9)
Water(BzGP) GAGB-2 (induce)	19.8(18.3)	14.7(13.3)	22.0(20.0)	11.8(10.0)	5.6(4.8)	−30.2(−35.0)	36.7(33.3)

[a] The energies are given in kcal/mol. Each simulation run involved 21 frames, each 20 ps. The first 10% simulation data in each run was excluded from the FEP/US calculations. $\Delta g^{\ddagger}_1$, ΔG_1, $\Delta g^{\ddagger}_2$, ΔG_2, $\Delta g^{\ddagger}_3$ and ΔG_3 are defined in figure 5 (see Fig. 5 for the definitions of these energies). The values in brackets are the corresponding experimental observed values, which are discussed in the results section. The notation induced designates calculations with induced dipoles.

Table 2

EVB reaction free energies and activation free energies for the different GAGB mechanisms in CPA [a].

	$\Delta g^{\ddagger}_1$	ΔG_1	$\Delta g^{\ddagger}_2$	ΔG_2	$\Delta g^{\ddagger}_3$	ΔG_3	$\Delta g^{\ddagger}_{cat}$(cal)	$\Delta g^{\ddagger}_{cat}$(exp)
Protein(pGluFF) GAGB-1	7.1	4.1	12.4	10.7	1.4	−28.6	16.5	14.0−16.0[b]
Protein(pGluFF) GAGB-2	16.9	11.5	8.6	1.8	0.0	−32.5	20.1	14.0–16.0[b]
Protein(BzGP) GAGB-1	7.1	1.8	11.8	−18.4	4.7	−32.6	13.6	16.0[c]
Protein(BzGP) GAGB-2	17.7	15.2	8.2	2.8	0.0	−63.1	23.4	16.0[c]
Protein(BzGP) GAGB-1(induce)	13.3	4.5	3.6	−36.2	14.8	−46.5	13.3	16.0[c]
Protein(BzGP) GAGB-2(induce)	15.7	9.0	19.9	4.8	0.0	−48.4	28.9	16.0[c]

[a] The energies are given in kcal/mol. Each simulation run involved 21 frames, each 20 ps. The first 10% simulation data in each run was excluded from the FEP/US calculations. $\Delta g^{\ddagger}_1$, ΔG_1, $\Delta g^{\ddagger}_2$, ΔG_2, $\Delta g^{\ddagger}_3$ and ΔG_3 are defined in figure 5. The notation induced designates calculations with induced dipoles.

[b] k_{cat} is estimated based on Rutter et al (1990) and Cho et al (2001).

[c] k_{cat} is taken from Rutter et al (1990), the estimated experimental error is ±2.7 kca/mol.

Table 3

EVB reaction free energies and activation free energies for the different GAGB mechanisms in the R127A mutation of CPA [a].

	$\Delta g^{\ddagger}_1$	ΔG_1	$\Delta g^{\ddagger}_2$	ΔG_2	$\Delta g^{\ddagger}_3$	ΔG_3	$\Delta g^{\ddagger}_{cat}$(cal)	$\Delta\Delta g^{\ddagger}_{cat}$(cal)	$\Delta\Delta g^{\ddagger}_{cat}$(exp)
R127A(BzGP) GAGB-1	9.0	7.2	17.0	−5.6	3.5	−38.1	24.2	10.6	6.0[b]
R127A(BzGP) GAGB-2	18.4	16.5	5.7	−2.8	0.0	−72.3	22.2	−1.2	6.0[b]
R127A(BzGP) GAGB-1(induce)	15.4	8.9	15.6	−15.6	20.7	−36.1	24.5	11.2	6.0[b]
R127A(BzGP) GAGB-2(induce)	19.9	8.1	7.9	−8.0	0.0	−43.2	16.0	−12.9	6.0[b]

[a] The energies are given in kcal/mol. Each simulation run involved 21 frames, each 20 ps. The first 10% simulation data in each run was excluded from the FEP/US calculations. $\Delta g^{\ddagger}_1$, ΔG_1, $\Delta g^{\ddagger}_2$, ΔG_2, $\Delta g^{\ddagger}_3$ and ΔG_3 are defined in figure 5. $\Delta\Delta g^{\ddagger}_{cat}$ corresponds to the effect of the mutation on $\Delta g^{\ddagger}_{cat}$. The notation induced designates calculations with induced dipoles.

[b] k_{cat} is taken from Rutter et al (1990), the estimated experimental error is ±5 kca/mol.

Table 4

EVB reaction free energies and activation free energies for the different GAGB mechanisms in CPA with uncharged zinc atom [a].

	$\Delta g^{\ddagger}_1$	ΔG_1	$\Delta g^{\ddagger}_2$	ΔG_2	$\Delta g^{\ddagger}_3$	ΔG_3	$\Delta g^{\ddagger}_{cat}$ (cal)	$\Delta\Delta g^{\ddagger}_{cat}$ (cal)	$\Delta\Delta g^{\ddagger}_{cat}$ (exp)
Zn(0)-CPA(BzGP) GAGB-1	19.7	18.8	16.8	9.6	12.1	10.4	35.6	22.0	NA[b]
Zn(0)-CPA(BzGP) GAGB-2	15.8	13.3	19.1	15.1	3.6	−39.7	32.4	9.0	NA[b]
Zn(0)-CPA(BzGP) GAGB-1(induce)	20.2	18.0	10.3	0.5	8.7	−3.0	28.3	15.0	NA[b]
Zn(0)-CPA(BzGP) GAGB-2(induce)	21.0	15.8	33.9	27.7	−0.7	−53.4	49.7	20.8	NA[b]

[a] The energies are given in kcal/mol. Each simulation run involved 21 frames, each 20 ps. The first 10% simulation data in each run was excluded from the FEP/US calculations. $\Delta g^{\ddagger}_1$, ΔG_1, $\Delta g^{\ddagger}_2$, ΔG_2, $\Delta g^{\ddagger}_3$ and ΔG_3 are defined in figure 5. $\Delta\Delta g^{\ddagger}_{cat}$ corresponds to the effect of zero charged zinc on $\Delta g^{\ddagger}_{cat}$. The notation induced designates calculations with induced dipoles.

[b] NA=not active, see Feinberg et al (1993).